IEEE Access
Multidisciplinary | Rapid Review | Open Access Journal

Received January 22, 2020, accepted January 30, 2020, date of current version February 14, 2020.

Digital Object Identifier 10.1109/ACCESS.2020.2971554

Inspection on Ball Bearing Malfunction by Chen-Lee Chaos System

CHIH-JER LIN[1], (Member, IEEE), XIAO-YI SU[1], KUAN-TING YU[2], BO-LIN JIAN[2], AND HER-TERNG YAU[2], (Member, IEEE)

[1]Graduate Institute of Automation and Technology, National Taipei University of Technology, Taipei 10608, Taiwan
[2]Department of Electrical Engineering, National Chin-Yi University of Technology, Taichung 41170, Taiwan

Corresponding author: Her-Terng Yau (pan1012@ms52.hinet.net)

This work was supported in part by the Ministry of Science and Technology of the Republic of China, Taiwan, under Contract MOST 108-2218-E-167-001 and Contract 108-2218-E-167-002.

ABSTRACT With the trend of Industry 4.0, the global machine tool industry is developing towards smart manufacturing. The ball bearing is a key component of the rotary axis of machine tool, and its functionality is to bear the external load on the axis as well as maintain the center position of the axis. A damaged bearing will result in abnormal vibration and noise, and thus will lead to the damage of the machine and produced workpieces. Therefore, inspection and identification of ball bearing failures is particularly important. This paper discusses the fault signals of ball bearings published by the Society for Machinery Failure Prevention Technology (MFPT) and creates a recognition model for the ball bearing state based on different fault states, and then we adopt two different approaches for feature extraction. The first approach implements Finite Impulse Response Filter (FIR) and Approximate Entropy (ApEn) to extract the signal features. The second approach utilizes the Chen-Lee chaotic system for analysis and takes its chaotic attractor as the feature of the state recognition. The comparison of model recognition accuracy for Back Propagation Neural Network (BPNN), Support Vector Machine (SVM), and K Nearest Neighbor (KNN) was conducted after acquiring the features through the two approaches in this paper. The results of the experiments in this paper show that both of the feature extraction approaches enable the state to be recognized easily. The Chen-Lee chaotic system with BPNN not only reaches 100% identification rate and it has the highest overall efficiency; it takes only 0.054 second to complete the feature extraction for 63 sets of data; this study is able to provide timely and precise solution for the failure of key mechanical components.

INDEX TERMS Ball bearing, back propagation neural network, support vector machine, fault detection, approximate entropy, Chen-Lee chaotic system.

I. INTRODUCTION

Ball bearings are carriers for supporting the mechanical rotating body, to reduce the coefficient of friction during rotation and ensure the rotational precision of mechanical components. Therefore, ball bearings are crucial parts of transmission equipment. If the equipped ball bearings are damaged, they may cause abnormal noise during machine operation or even cause the machine to stop operating which will affect the production capacity. The researchers focus on the implementation of malfunction inspection and analysis without stopping the machine operation in order to reduce the possible loss of production cost due to the damage of ball bearings. Many researches have conducted on malfunction diagnosis and lifespan analysis of ball bearing [1]–[3] in the running state. However, the ISO [4] stipulated industrial standards for ball bearing state make the definition of the ball bearing state much clearer; most researches are dedicated to measure the current on the loading driver for analysis [5], [6], the audio frequency variation during ball bearing operation [7], [8], abnormal temperature [9], [10] variation in ball bearing, and the feature of vibration variation generated during ball bearing operation [11], [12]. Most of the research methods discuss the amplitude of frequency spectrum based on converting the time-domain signal to the frequency-domain signal [13], [14]. For example, the Fast Fourier transform (FFT) [15], [16] and wavelet transform [17], [18] are applied for feature extraction; however, the fast Fourier transform is not able to precisely describe the local feature of a signal, and the wavelet

The associate editor coordinating the review of this manuscript and approving it for publication was Ludovico Minati.

transform has difficulty to process in real time due to a large amount of computations; and thus the efficiency and accuracy of signal pre-process will be the key for technology advancement in this stage.

Therefore, this paper discusses the fault signals of ball bearings published by the Society for Machinery Failure Prevention Technology (MFPT) and adopts two different approaches for feature extraction. The first approach implements Finite Impulse Response Filter (FIR) [19]–[21] for signal decomposition and Approximate Entropy (ApEn) [22], [23] for feature extraction. The second approach utilizes the Chen-Lee chaotic system [24]–[26] for analysis and takes its chaotic attractor as the feature of the state recognition. The feature data extracted from the two approaches are substituted into the Back Propagation Neural Network (BPNN) [27], [28] for model training, testing, and classification of identification rate. The classification of accuracy rate and overall efficiency for the Support Vector Machine (SVM) [29], [30] and K Nearest Neighbor (KNN) [31], [32] are then compared for further discussion.

II. METHODS

A. EXPERIMENTAL EQUIPMENT

The simulation data used in this essay are the analytic outcomes from the database of malfunction signals of ball bearing provided by MFPT, wherein the ball bearing equipped in the experimental equipment in the database is developed and manufactured by RBC Bearings Incorporated. Please refer to TABLE 1 for the detailed structural parameters of the ball bearing, of which the sampling frequencies of vibration signals are 97,656Hz and 48,828Hz. TABLE 2 is the detailed malfunction specifications of a ball bearing, including load under normal status, load by outer ring malfunction, as well as load by inner ring malfunction. The software for verification is Matlab 2019a, where the toolbox used is Machine Learning Toolbox 11.5, Deep Learning Toolbox 12.1 and Neural Network Training Toolbox.

TABLE 1. Ball bearing parameters.

Type	Parameters
Roller Dia.	0.235(inch)
Pitch Dia.	1.245(inch)
Number of Element	8
Contact Angle	0°

TABLE 2. Malfunction type of ball bearing.

Type	Parameters
Sampling Frequency	97,656/48,828 (Hz)
Load of Normal Status	270 (Pounds)
Load of Outer Ring Malfunction	25/50/100/150/200/250/300 (Pounds)
Load of Inner Ring Malfunction	0/50/100/150/200/250/300 (Pounds)

B. EXPERIMENTAL STRUCTURE

The designed experimental flow of this study is as FIGURE 1. In the beginning, various status of a bearing in the database acquired by the accelerometer will be classified. Original sampling frequency of the signals under normal status is 97,656Hz, six seconds for each sampling, therefore the length of data point is 585,936 and there are three data (585936×3). Original sampling frequency of the signals of outer ring status is 48,828Hz, three seconds for each sampling, therefore the length of data point is 146,484 and there are seven datum ($146{,}484 \times 7$). Original sampling frequency of the signals of inner ring status is 48,828Hz, three seconds for each sampling, therefore the length of data point is 146,484 and there are seven datum ($146{,}484 \times 7$). In order to unify all the data lengths as well as numbers in regard to each status, we process the original bearing status by reducing the frequencies and creating the segments, while we do not use any repeated sample during signal processing. As a result, there are 48,828 data points in length by respective segmentation and 21 data for three different status ($48{,}828 \times 21 \times 3$), *i.e.* normal status, outer ring breakdown and inner ring breakdown, to be the classification resources of normal-stated signals in this study. As shown in TABLE 3.

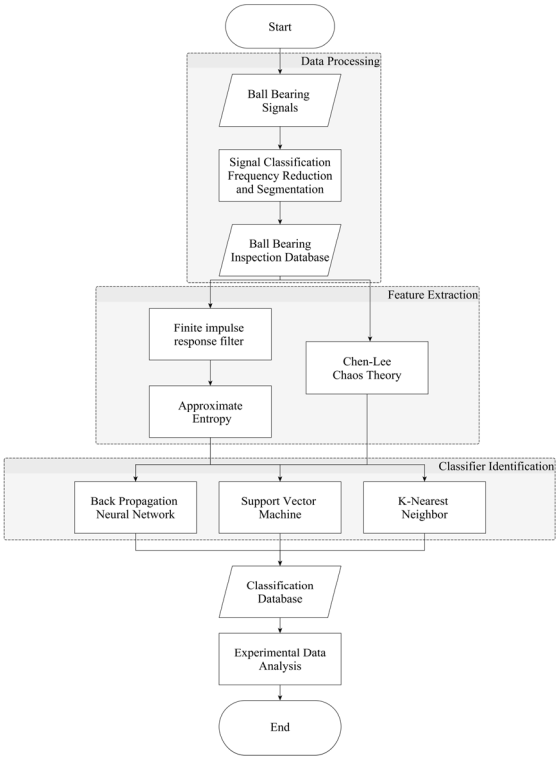

FIGURE 1. Flow chart of experiment.

TABLE 3. Number of data records in three different states.

State	Number of data records
Normal	21
Outrace fault	21
Inner race fault	21

The damaged parts of the bearing are usually the inner race, outrace and the ball. The causes of damage are due to the increased vibration and generated heat which are closely related to the circumstance of vibration signal of the bearing. The obtained vibration signals are quite different as the damage spots of the bearing are different. The fault characteristic frequency formula refers to [33]. The formula is shown in (1) ∼ (3).

$$f_i = \frac{N}{2}\left(1 + \frac{d_b}{D}\cos\alpha\right) f_r \tag{1}$$

$$f_o = \frac{N}{2}\left(1 - \frac{d_b}{D}\cos\alpha\right) f_r \tag{2}$$

$$f_b = \frac{D}{d_b}\left(1 - \left(\frac{d_b}{D}\cos\alpha\right)^2\right) f_r \tag{3}$$

where Formula (1) is the characteristic frequency of inner race fault, Formula (2) is the characteristic frequency of outrace fault, and Formula (3) is the characteristic frequency of ball fault. In the above three formulas, N represents the number of rolling element, d_b represents the Roller Dia, D represents the Pitch Dia, α represents the Contact angle, and f_r represents the rotation frequency of the bearing; the unit is rotor speed/minute.

In this essay, FIR is collocated with ApEn and Chen-Lee chaos system, creating two distinct methods to perform feature extraction. The first one is to use FFT to transform the time-domain into frequency-domain of the vibration signals by the three status of a ball bearing, and then we can use the frequency response graph to judge the wave bands with the features of each bearing status to implement band-pass filtration, where the filtration scope is from 105Hz to 10,200Hz. Therefore, we can keep these wave bands of various status for feature extraction by ApEn subsequently. The filtered signals will then be adopted with ApEn to obtain the features from three different status, for this reason the number of feature which can process 63 signals is 63. The second method is to create the nonlinear feature mapping of the vibration signals in time-domain of the three status, and then to make the deduction between rated signals and test signals to obtain the chaotic dynamic error distribution mapping as well as chaotic dynamic error centroid coordinates to be our identification features. After analyzing and comparing via experiment, we use the x coordinate of the chaotic centroid to be the feature to identify bearing status, as a result, both the numbers of datum and features are as the same as the first method. At last of the experiment, we use BPNN, SVM and K-NN to classify identification, as well as compare the time spent on feature extraction, training and testing.

C. FINITE IMPULSE RESPONSE FILTER

Finite impulse response filter, of which the abbreviation is FIR, is one member of the digital filters. Because the response for an impulse input signal in FIR is approximately 0, this kind of response is rather limited, where its mission is to change the spectrum of the inputted signals via computation. FIR has several merits: finite long-term output digital signals are subject to the limitation by inputting the digital signals, being easier to optimize than Infinite Impulse Response Filter (IIR) [34], as well as that all the polar coordinates are relatively stable within the unit circle after Z transformation, where the relations between input-output are represented as a difference equation (1) shown as below:

$$y(n) = \sum_{k=0}^{K} b_k x(n-k) \tag{4}$$

wherein $x(n)$ is the outer input signal, $y(n)$ is FIR output signal, K is the order of filter, and b_k is filter impulse response that can also represent the filter coefficient. This study is to perform band-pass filtration ranged from 105Hz to 10,200Hz among all the signals.

D. APPROXIMATE ENTROPY

Approximate Entropy (ApEn) is a solution to extract features. It is a complexity index, which can reflect if there is any similar outcome or condition within the same data segments. If there is any abnormality in the datum, we can clearly see the statistical variation on out conclusion. So far this method can be introduced into a certain researches with analysis on complexity of frequency band, as for the descriptions of ApEn are as below [35], [36]:

Set the original data as $X(n) = x(1), x(2) \cdots x(N)$,wherein is the total number of the data points, and sequence $\{x(i)\}$ is sequentially composed by m-dimensional vector $\{x(i)\}$; i.e. a set of m-dimensional vector composed of a continuous sequence is shown as (2):

$$X(i) = [x(i), x(i+1), \ldots, x(i+m-1)], \quad i = 1, 2, \ldots N-m+1 \tag{5}$$

Define the distance $d\,|X(i), X(j)|$ between $X(i)$ and $X(j)$ as the maximum distance of each correspondent element as (3):

$$d[X(i), X(j)] = \max_{k=0\to m-1}[|x(i+k) - x(j+k)|] \tag{6}$$

wherein $1 \le i \le N-m+1$ and $1 \le j \le N-m+1$.

Given noise filtration coefficient r, that satisfies the data numbers of the conditions $d[x(i), x(j)] \le r$. Comparing the sum of the value thereof with $N-m+1$, then we can obtain the proportion of the similar numbers by total numbers, which is defined as the equation (4):

$$C_i^m(r) = \frac{1}{N-M+1}\sum\nolimits_{i=1, i\neq j}^{N-m+1} |d[x(i) - x(j)]|$$

$$wherein\ d(i,j) = \begin{cases} 1, & |d[x(i) - x(j)]| \le r \\ 0, & |d[x(i) - x(j)]| \ge r \end{cases} \tag{7}$$

Afterwards we take the logarithm of $C_i^m(r)$ to calculate the averages among all the i of $C_i^m(r)$ and record them as $\phi^m(r)$, which is defined as (5):

$$\phi^m(r) = \frac{1}{N-m+1}\sum_{i=1}^{N-m+1} \ln C_i^m(r) \tag{8}$$

Set that the dimension m plus 1 to become $m+1$ then we can acquire $C_i^{m+1}(r)$ and $\phi_i^{m+1}(r)$, thereupon the value of ApEn can be calculated through (6):

$$ApEn(m,r) = \lim_{N\to\infty}\left[\phi^m(r) - \phi^{m+1}(r)\right] \tag{9}$$

Because the actual data points N are impossible to be infinite, we change (6) to (7):

$$ApEn(m,r,N) = \phi^m(r) - \phi^{m+1}(r) \tag{10}$$

E. CHEN-LEE CHAOS SYSTEM DYNAMIC ERROR

Chaos system is a part of the non-linear system theories, of which one of it features is very sensitive to any minor variation of inputted signals. If the input changes even if only a little, the correspondent output will significantly change. Also, the chaos system possesses strange attractor, the outputted movement status will be a motion track with order but no cycle. The Chen-Lee chaos system is designed for a dynamic system, used as the non-linear transformation mapping, wherein we utilize both the coordinates of chaotic dynamic error mapping and chaotic dynamic error centroid as the identification features. The Chen-Lee dynamic equation is shown as (8).

$$\begin{cases} \dot{x} = -yz + \alpha x \\ \dot{y} = xz + \beta y \\ \dot{z} = \dfrac{1}{3}xy + \gamma z \end{cases} \tag{11}$$

In order to obtain the Chen-Lee chaos system dynamic error, we modify the equation above as the formats of rated ideal signal system and test signal system, which are shown as (9) and (10).

$$\begin{cases} \dot{x}_m = -y_m z_m + \alpha x_m \\ \dot{y}_m = x_m z_m + \beta y_m \\ \dot{z}_m = \dfrac{1}{3}x_m y_m + \gamma z_m \end{cases} \tag{12}$$

$$\begin{cases} \dot{x_s} = -y_s z_s + \alpha x_s \\ \dot{y_s} = x_s z_s + \beta y_s \\ \dot{z_s} = \dfrac{1}{3}x_s y_s + \gamma z_s \end{cases} \tag{13}$$

whereas the system dynamic error is the reduction between rated ideal signal system and test signal system.

For the convenience for the reduction of these two systems, we can modify these two equations above to matrix format [24], which are represented as (11) and (12):

$$\begin{bmatrix} \dot{x_m} \\ \dot{y_m} \\ \dot{z_m} \end{bmatrix} = \begin{bmatrix} \alpha & 0 & -y_m \\ 0 & \beta & x_m \\ 0 & \dfrac{1}{3}x_m & \gamma \end{bmatrix} \begin{bmatrix} x_m \\ y_m \\ z_m \end{bmatrix} \tag{14}$$

$$\begin{bmatrix} \dot{x_s} \\ \dot{y_s} \\ \dot{z_s} \end{bmatrix} = \begin{bmatrix} \alpha & 0 & -y_s \\ 0 & \beta & x_s \\ 0 & \dfrac{1}{3}x_s & \gamma \end{bmatrix} \begin{bmatrix} x_s \\ y_s \\ z_s \end{bmatrix} \tag{15}$$

This study seeks to introduce the concept of discrete signal processing, therefore the vibration signals in time-domain (chaotic dynamic) of both rated ideal signal system and test signal system are shown as below [24]–[26], [37]–[39]:

$$n[i] = \{n[1], n[2], n[3]\cdots n[i]\} \tag{16}$$

$$t[i] = \{t[1], t[2], t[3]\cdots t[i]\} \tag{17}$$

Following the idea described in the preceding paragraphs, it is easy to define the parameters of rated signal system (11) as $x_m[i] = n[i+1]$, $y_m[i] = n[i+2]$ and $z_m[i] = n[i+3]$, as well as define the parameters of test signal system (12) as $x_s[i] = t[i+1]$, $y_s[i] = t[i+2]$ and $z_s[i] = t[i+3]$. In order to obtain the chaos system dynamic error, we deduct (11) from (12). The equation of chaos system dynamic error is shown as (14).

$$\begin{bmatrix} \dot{e}_1[i] \\ \dot{e}_2[i] \\ \dot{e}_3[i] \end{bmatrix} = \begin{bmatrix} \alpha & 0 & 0 \\ 0 & \beta & 0 \\ 0 & 0 & \gamma \end{bmatrix} \begin{bmatrix} e_1 \\ e_2 \\ e_3 \end{bmatrix} + \begin{bmatrix} -e_2 e_3 \\ e_1 e_3 \\ \dfrac{1}{3}e_1 e_2 \end{bmatrix} \tag{18}$$

In (15), $e_1[i] = x_m[i] - x_s[i]$, $e_2[i] = y_m[i] - y_s[i]$ and $e_3[i] = z_m[i] - z_s[i]$, wherein α, β and γ are the system parameters and satisfy $\alpha > 0$, $\beta < 0$ and $0 < \alpha < (-\beta + \gamma)$ to guarantee that the system features strange attractor[40]. After the comparison by the experiment in this study, we will use the x coordinate of the chaotic centroid as the feature physical quantity when we analyze the malfunction of a ball bearing.

F. BACK PROPAGATION NEURAL NETWORK

Back Propagation Neural Network (BPNN) is composed of Multi-Layer Perceptron (MLP) [41], [42] and Error Back Propagation (EBP or BP) [43], where the fundamental theorem is use Gradient Descent [44] to minimize the error function. Back Propagation Neural Network is a supervised learning network, which is also the most representative and widely applicable one among all the neural networks.

This paper utilizes BPNN as the main classifier and the basic structure includes Input Layer, Hidden Layer and Output Layer. The setting for the amount of neuron in hidden layer will highly affect the diagnostic accuracy rate. This paper adopts the BPNN to provide features to the input layer after preprocessing the signals. The output of the output layer is a label for the ball bearing state provided by the database, so that the training of the model can be completed and the subsequent identification can be verified.

BPNN is as a typical MLP, of which the different layer will be connected through weight and error. Input of the next layer is the processed outcome from the previous layer through nonlinear activation function, and the formula is as (16):

$$S_j = f\left(\sum_{i=0}^{m-1} w_{ij}x_i + b_j\right) \tag{19}$$

wherein S_j is the inputted value of the j^{th} hidden layer, whilst w_{ij} is the weight to connect each process unit of different

layers, x_i is the inputted value of the i^{th} unit, and b_j is the bias. $f(x)$ is an activation function named as Sigmoid, which is defined as (17):

$$f(x) = \frac{1}{1 - e^{-x}} \tag{20}$$

When there is an error between expected value and actual value, BPNN will feedback the error layer by layer to both the weight and bias of the modification model of each hidden layer, and then re-deliver the inputted value of training datum to the next layer according to the calculation of the whole new weight and bias of each layer, where this process will be repeatedly exercised until the error value is acceptable. In order to reduce the difference between the inputted value and target value of the network, the error modification thereof is shown as (18):

$$E = \frac{1}{2} \sum_{i \in outputs} (y_{(i)} - \hat{y}_{(i)})^2 \tag{21}$$

Wherein $y_{(i)}$ is the actual value and $\hat{y}_{(i)}$ is the expected value.

III. EXPERIMENTAL OUTCOMES AND DISCUSSIONS

A. FEATURE EXTRACTION OUTCOMES OF FIR AND APEN

First, the time-domain signals of the normal, outrace fault and inner race fault are shown on the left of FIGURE 2 (a) to (c) for the conversion of frequency-domain and frequency-domain through FFT. The feature band of each bearing state can be determined according to the frequency-domain response map. On the right of FIGURE 2 (d) to (f), it can be seen that the feature band in normal state is 9889 to 10140 Hz, the feature band in outrace fault is 1121 to 1281 Hz, and the feature band in inner race fault is 4525 to 4774 Hz. The Bandpass filter is implemented to filter all signals with a filtering range of 105 to 10200 Hz for subsequent feature extraction and classifier recognition. The filtering range in the frequency-domain is indicated in a red box on the right of FIGURE 2 (d) to (f).

All the signals which have been filtered by band-pass filter will be adopted with ApEn for feature extraction, and the proportion of the similar numbers by total numbers can be obtained through the computation and reduction of order by ApEn, as well as that we can clearly see the change upon statistical outcomes. FIGURE 3 respectively represent the signal maps of data size after feature extraction by ApEn for normal status, outer ring malfunction and inner ring malfunction; also, we can see in FIGURE 3 that all the features extracted are independent of each other by each status, and all the sizes and distribution areas of each status can be easily identified. After calculating by ApEn as show in Table 4, the standard deviation and mean value of each state, proving that the features independently of each other. In TABLE 5, the T-test was used to calculate the significance between each state after ApEn is applied.

B. CHEN-LEE CHAOS SYSTEM NONLINEAR FEATURE MAPPING RESULTS

If we exercise non-linear feature mapping upon the time-domain map of the three bearing status in FIGURE 2,

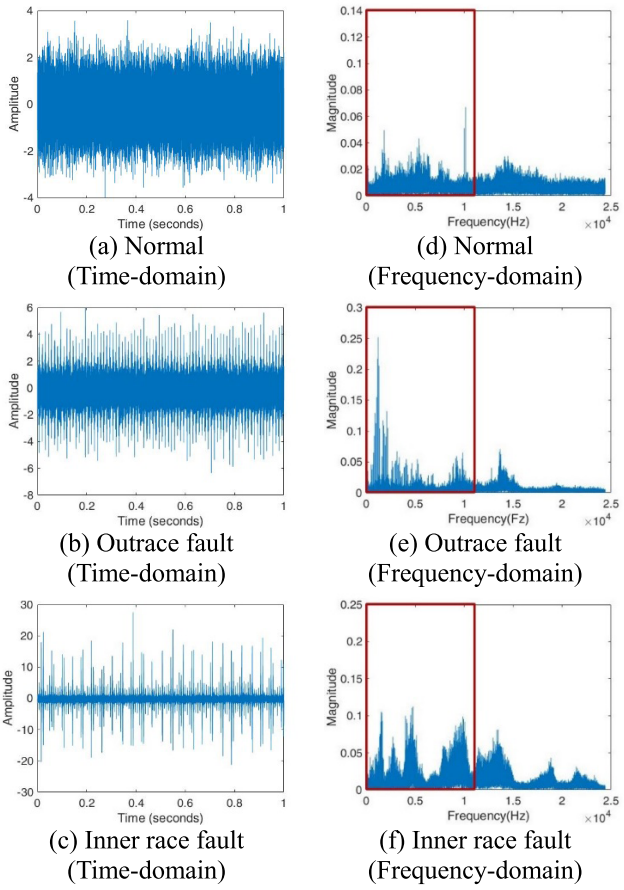

FIGURE 2. Time-domain and frequency-domain map of three bearing.

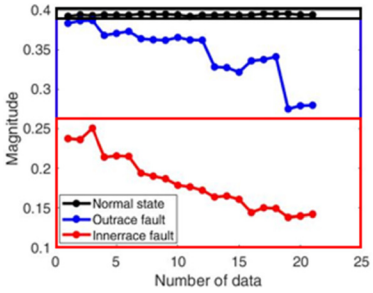

FIGURE 3. Feature distribution map of three bearing status by ApEn.

TABLE 4. After calculating by ApEn, the standard deviation and mean value of each state are as follows.

	Normal	Outrace fault	Inner race fault
Means	0.3939	0.3462	0.1812
SDs	0.0009	0.0344	0.0348

TABLE 5. Significance between each state after ApEn is applied (using the T-test).

	Normal state to Outrace fault	Outrace fault to Inner race fault	Inner race fault to Normal state
P-value	0.153×10^{-6}	2.19×10^{-18}	7.92×10^{-28}

we can divide the status features as being independent in high efficiency through the sensitivity upon the minor variation of chaos system to signals. From FIGURE 4 (a) to (c) we can see the graph distribution and size difference between the maps of normal status, outer ring malfunction and inner ring malfunction after analyzing them by the Chen-Lee chaos system. Through the experiment and comparison in this study, we take the coordinate of chaos centroid to be the physical quantity for ball bearing malfunction analyses. From FIGURE 5 there

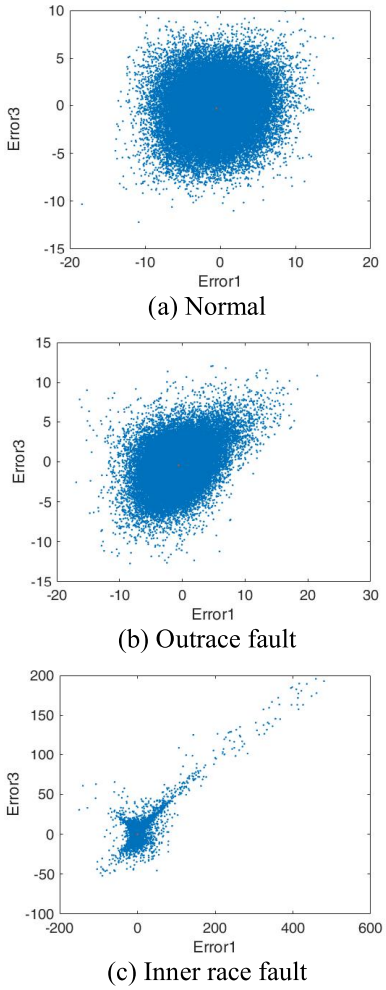

FIGURE 4. Chen-Lee chaos system dynamic error distribution map.

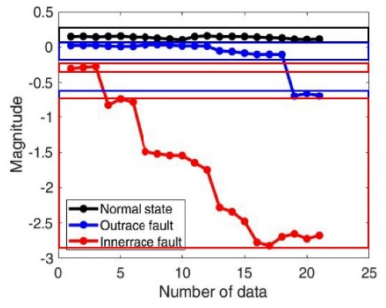

FIGURE 5. Chen-Lee chaos system feature distribution maps of three bearing status.

are the feature extraction maps of normal status, outer ring malfunction and inner ring malfunction after analyzing by the Chen-Lee chaos system.

FIGURE 5 shows the distributional proportion map of combining the feature signals of the three bearing status, and we can understand that the data value from the 18th data to the 21th data of outer ring malfunction is approximate to the one calculated from the 1st data to the 6th data of inner ring malfunction, which might cause the subsequent misjudgment of identification by the classifier. After calculating by Chen-Lee Chaos System as show in Table 6, the standard deviation and mean value of each state. proving that the features independently of each other. In III-C, the T-test was used to calculate the significance between each state after the Chen-Lee Chaos System is applied.

TABLE 6. After calculating by Chen-Lee Chaos System, the standard deviation and mean value of each state are as follows.

	Normal	Outrace fault	Inner race fault
Means	0.1379	-0.1102	-1.7212
SDs	0.0173	0.2469	0.9012

TABLE 7. Significance between each state after Chen-Lee Chaos System is applied (using the T-test).

	Normal state to Outrace fault	Outrace fault to Inner race fault	Inner race fault to Normal state
P-value	4.304×10^{-5}	1.077×10^{-9}	9.572×10^{-12}

C. BPNN IDENTIFICATION RESULTS AND COMPARISON OF OTHER CLASSIFICATION MODELS

The inner parameter configuration of BPNN does not have any certain accordance and specification. As a result, this study is to fix the parameters for training function, neural number and training data number. Also, the training function introduced in this study is Trainscg, and GPU is used here to assist the computation; neural number is set as 1,000 and the data training volume is 90% to perform the test on the 10% volume. Under the same parameter conditions, we implement the training upon the datum with two different pre-processing to compare the time spent as well as the difference of identification rates between the two data pre-processing measures. Furthermore, we are to compare the datum of which the features are not yet extracted by BPNN, SVM and K-NN.

It can be discovered form TABLE 8 and TABLE 10 that the feature extraction time for the proposed Chen-Lee Chaos system in this paper is much faster than the time for the FIR with ApEn. On the basis of original data comparison, we can see that the two proposed approaches for feature extraction in this paper are able to increase the identification rate in all three classifiers as well as reduce the model training time and testing time. Among these three classifiers, the BPNN has less testing time under the circumstances without losing its recognition accuracy. Both feature extraction methods as well as a randomly selected raw signal which was used to calculate the mean and standard deviation with the results

TABLE 8. Spend time comparison between three classifier models.

Classifier	Method	Feature Extraction Time(seconds)	Training Time (seconds)	Test Time(seconds)
BPNN	Original Data	0	267.80	1.889
	FIR+ApEn	3197.95	5.32	0.106
	Chen-Lee Chaos System	0.545	5.715	0.114
SVM	Original Data	0	335.4	42.3
	FIR+ApEn	3197.95	5.654	0.134
	Chen-Lee Chaos System	0.545	5.062	0.86
K-NN	Original Data	0	334.1	36.77
	FIR+ApEn	3197.95	1.122	0.147
	Chen-Lee Chaos System	0.545	0.97	0.145
Note: Filtering range of FIR filter is between 105 and 10200Hz, the number of hidden layers in the BPNN model is 100, and the training function is trainscg.				

TABLE 9. Standard deviations and means of the signal after feature extraction.

	Original Data	FIR+ApEn	Chen-Lee Chaos System
Means	-0.1399	0.3939	0.1379
SDs	0.8531	0.000902	0.0173

TABLE 10. 10 identification rate comparison between three classifier models (10-fold cross-validation).

Classifier	Method	Data Training Proportion (%)	Data Testing Proportion (%)	Identification Rate(%)
BPNN	Original Data	80	10	38.3
	FIR+ApEn			100
	Chen-Lee Chaos System			100
SVM	Original Data	80	10	65.1
	FIR+ApEn			100
	Chen-Lee Chaos System			100
K-NN	Original Data	80	10	65.1
	FIR+ApEn			100
	Chen-Lee Chaos System			100

shown in TABLE 9. In addition, we also compare with other research paper using the same database. A research paper published by David Verstraete uses STFT for the time and frequency conversion [45], and implements an in-depth learning network for identification as well as compares the classification of accuracy rate. The identification rate is similar to the results obtained in this paper which is close to 100%; however, the classifier used in the research paper published by David Verstraete is an in-depth learning network with a longer training and testing time, and it also has longer feature extraction time of the Short-time Fourier Transform. In general, the proposed approach in this paper has higher efficiency and thus it has the advantage of system construction in a real time, as well as the possibility of being extended to the micro-processing systems.

IV. CONCLUSION

This study seeks to propose a judgement system on ball bearing malfunction status with efficiency as well as robust classification. Also, we aim at the open datum in regard to a ball bearing released by Machinery Failure Prevention Technology, trying to exercise feature extraction and mapping by using two signal pre-processing methods and then using the three classification models to classify and diagnose the ball bearing status, and at the same time comparing the precision and overall computational efficiency between the methods that have been described as above. Therefore, we can come to the conclusion in this essay that although the colocation of FIR and ApEn has a very tremendous effect on feature extraction, as well as the features extracted thereof are all relatively independent in each status, it needs 3,197.95 seconds to pre-process the signals. Out of the cause of effectiveness, it is not appropriate to be introduced into a real-time diagnostic system. As a result, in order to solve the efficiency problem caused by signal pre-processing, we adopt the Chen-Lee chaos system as our malfunction diagnosis measure to implement nonlinear feature mapping for the vibration signals of a ball bearing. Through the sensitivity upon the minor variation of the signals by this chaos system, we can make each feature status independent, where the precision of classification and total time spent can be referred in TABLE 8 and TABLE 10 that all the precision rates of every classification model are 100%, while the total time spent on pre-processing is 0.545 seconds. Comparing with the method regarding the collocation of FIR and ApEn, not only the precision rate of Chen-Lee chaos system holds at a good quality, but is also better than the former one in computational efficiency. It has been therefore proved that Chen-Lee chaos system is highly effective and practical for the diagnosis on ball bearing status, and is very promising to be applied in the real-time diagnosis system in the future.

REFERENCES

[1] Y. Qian and R. Yan, "Remaining useful life prediction of rolling bearings using an enhanced particle filter," *IEEE Trans. Instrum. Meas.*, vol. 64, no. 10, pp. 2696–2707, Oct. 2015.

[2] J. Zhu, N. Chen, and W. Peng, "Estimation of bearing remaining useful life based on multiscale convolutional neural network," *IEEE Trans. Ind. Electron.*, vol. 66, no. 4, pp. 3208–3216, Apr. 2019.

[3] M. Devaney and L. Eren, "Detecting motor bearing faults," *IEEE Instrum. Meas. Mag.*, vol. 7, no. 4, pp. 30–50, Dec. 2004.

[4] A. Bewoor and S. Kulkarni, "Interoperability of international standards, condition monitoring methods and research models for bearing fault: An integrated approach," *Procedia Manuf.*, vol. 22, pp. 982–989, 2018.

[5] M. Blodt, P. Granjon, B. Raison, and G. Rostaing, "Models for bearing damage detection in induction motors using stator current monitoring," *IEEE Trans. Ind. Electron.*, vol. 55, no. 4, pp. 1813–1822, Apr. 2008.

[6] Q. Han, Z. Ding, X. Xu, T. Wang, and F. Chu, "Stator current model for detecting rolling bearing faults in induction motors using magnetic equivalent circuits," *Mech. Syst. Signal Process.*, vol. 131, pp. 554–575, Sep. 2019.

[7] T. Noreesuwan and B. Suksawat, "Investigation of sound signal for ball bearing monitoring based on various tolerance fits," in *Proc. 11th Int. Conf. Control, Autom. Syst.*, 2011, pp. 482–485.

[8] S. Lu, X. Wang, Q. He, F. Liu, and Y. Liu, "Fault diagnosis of motor bearing with speed fluctuation via angular resampling of transient sound signals," *J. Sound Vib.*, vol. 385, pp. 16–32, Dec. 2016.

[9] B. Li, S.-L. Wang, and D. Yang, "Stress and fatigue life monitoring of high temperature bearing elements based on the solution of inverse conduction problem," in *Proc. Int. Conf. Condition Monit. Diagnosis*, 2008, pp. 184–187.

[10] O. Magdun, Y. Gemeinder, and A. Binder, "Investigation of influence of bearing load and bearing temperature on EDM bearing currents," in *Proc. IEEE Energy Convers. Congr. Expo.*, Sep. 2010, pp. 2733–2738.

[11] P. Nivesrangsan and D. Jantarajirojkul, "Bearing fault monitoring by comparison with main bearing frequency components using vibration signal," in *Proc. 5th Int. Conf. Bus. Ind. Res. (ICBIR)*, 2018, pp. 292–296.
[12] S. M. Khot and S. Gurav, "Investigation of effect of surface failures on inner and outer race of bearing on vibration spectrum," in *Proc. Int. Conf. Nascent Technol. Eng. Field (ICNTE)*, Jan. 2015, pp. 1–4.
[13] Y. Yufeng, Y. Jianwei, C. Guoqiang, and Y. Dechen, "Fault diagnosis of rolling bearing based on wavelet packet and Fourier analysis," in *Proc. Int. Conf. Comput. Aspects Social Netw.*, Sep. 2010, pp. 703–706.
[14] J. Wang, Z. Mo, H. Zhang, and Q. Miao, "A deep learning method for bearing fault diagnosis based on time-frequency image," *IEEE Access*, vol. 7, pp. 42373–42383, 2019.
[15] H. Chen and H. Pu, "Fault analysis of induction motor based on discrete fractional Fourier transform," in *Proc. Int. Symp. Comput., Consum. Control (IS3C)*, 2016, pp. 69–72.
[16] C. Macinnes, "FFT-based joint bearing estimation," *IEEE J. Ocean. Eng.*, vol. 27, no. 4, pp. 774–779, Oct. 2002.
[17] L. Eren, Y. Cekic, and M. J. Devaney, "Motor condition monitoring by empirical wavelet transform," in *Proc. 26th Eur. Signal Process. Conf. (EUSIPCO)*, Sep. 2018, pp. 196–200.
[18] Z. Huo, Y. Zhang, P. Francq, L. Shu, and J. Huang, "Incipient fault diagnosis of roller bearing using optimized wavelet transform based multi-speed vibration signatures," *IEEE Access*, vol. 5, pp. 19442–19456, 2017.
[19] B. N. Mohapatra and R. K. Mohapatra, "Performance analysis on frequency response of finite impulse response filter," *Procedia Comput. Sci.*, vol. 79, pp. 729–736, Jan. 2016.
[20] Y. A. Grebenko and R. I. Polyak, "Choosing a FIR filter order for the linearization of an analog LPF phase response," in *Proc. Syst. Signal Synchronization, Gener. Process. Telecommun. (SYNCHROINFO)*, Jul. 2018, pp. 1–3.
[21] W.-L. Chu, M.-W. Huang, B.-L. Jian, and K.-S. Cheng, "Analysis of EEG entropy during visual evocation of emotion in schizophrenia," *Ann. Gen. Psychiatry*, vol. 16, p. 34, Dec. 2017.
[22] X. Gao, X. Yan, P. Gao, X. Gao, and S. Zhang, "Automatic detection of epileptic seizure based on approximate entropy, recurrence quantification analysis and convolutional neural networks," *Artif. Intell. Med.*, vol. 102, Jan. 2020, Art. no. 101711.
[23] Z. Junyi, Y. Chaoying, X. Zhiwei, L. Yue, and W. Zhiqi, "A method for identifying the fault current of DC traction power supply system based on EMD approximate entropy," in *Proc. Int. Conf. Green Energy Appl. (ICGEA)*, Mar. 2017, pp. 18–21.
[24] H.-T. Yau, S.-Y. Wu, C.-L. Chen, and Y.-C. Li, "Fractional-order chaotic self-synchronization-based tracking faults diagnosis of ball bearing systems," *IEEE Trans. Ind. Electron.*, vol. 63, no. 6, pp. 3824–3833, Jun. 2016.
[25] H.-T. Yau, C.-C. Wang, J.-Y. Chang, and X.-Y. Su, "A study on the application of synchronized chaotic systems of different fractional orders for cutting tool wear diagnosis and identification," *IEEE Access*, vol. 7, pp. 15903–15911, 2019.
[26] B.-L. Jian, C.-C. Wang, J.-Y. Chang, X.-Y. Su, and H.-T. Yau, "Machine tool chatter identification based on dynamic errors of different self-synchronized chaotic systems of various fractional orders," *IEEE Access*, vol. 7, pp. 67278–67286, 2019.
[27] W. Wu, G. Feng, Z. Li, and Y. Xu, "Deterministic convergence of an online gradient method for BP neural networks," *IEEE Trans. Neural Netw.*, vol. 16, no. 3, pp. 533–540, May 2005.
[28] D. J. Hemanth, J. Anitha, and L. H. Son, "Brain signal based human emotion analysis by circular back propagation and Deep Kohonen Neural Networks," *Comput. Electr. Eng.*, vol. 68, pp. 170–180, May 2018.
[29] G. Ji, P. Han, and Y. Zhai, "Wind speed forecasting based on support vector machine with forecasting error estimation," in *Proc. Int. Conf. Mach. Learn. Cybern.*, 2007, pp. 2735–2739.
[30] X. Li, Y. Yang, H. Pan, J. Cheng, and J. Cheng, "A novel deep stacking least squares support vector machine for rolling bearing fault diagnosis," *Comput. Ind.*, vol. 110, pp. 36–47, Sep. 2019.
[31] J. Gou, W. Qiu, Z. Yi, X. Shen, Y. Zhan, and W. Ou, "Locality constrained representation-based K-nearest neighbor classification," *Knowl.-Based Syst.*, vol. 167, pp. 38–52, Mar. 2019.
[32] D. Ha, U. Ahmed, H. Pyun, C.-J. Lee, K. H. Baek, and C. Han, "Multi-mode operation of principal component analysis with k-nearest neighbor algorithm to monitor compressors for liquefied natural gas mixed refrigerant processes," *Comput. Chem. Eng.*, vol. 106, pp. 96–105, Nov. 2017.
[33] A. Rai and S. Upadhyay, "A review on signal processing techniques utilized in the fault diagnosis of rolling element bearings," *Tribol. Int.*, vol. 96, pp. 289–306, Apr. 2016.
[34] T. Tarumi, G. W. Small, R. J. Combs, and R. T. Kroutil, "Infinite impulse response filters for direct analysis of interferogram data from airborne passive Fourier transform infrared spectrometry," *Vib. Spectrosc.*, vol. 37, no. 1, pp. 39–52, Jan. 2005.
[35] L. Huang, Y. Wang, J. Liu, and J. Wang, "Approximate entropy of EEG as a measure of cerebral ischemic injury," in *Proc. 26th Annu. Int. Conf. IEEE Eng. Med. Biol. Soc.*, Apr. 2005, pp. 4537–4539.
[36] H. Zhang and S.-S. He, "Analysis and comparison of permutation entropy, approximate entropy and sample entropy," in *Proc. Int. Symp. Comput., Consum. Control (IS3C)*, Dec. 2018, pp. 209–212.
[37] F.-C. Gu, H.-T. Yau, and H.-C. Chen, "Application of chaos synchronization technique and pattern clustering for diagnosis analysis of partial discharge in power cables," *IEEE Access*, vol. 7, pp. 76185–76193, 2019.
[38] C.-L. Kuo, C.-H. Lin, H.-T. Yau, and J.-L. Chen, "Using self-synchronization error dynamics formulation based controller for maximum photovoltaic power tracking in micro-grid systems," *IEEE J. Emerg. Sel. Topics Circuits Syst.*, vol. 3, no. 3, pp. 459–467, Sep. 2013.
[39] H.-T. Yau, Y.-C. Li, C.-L. Chen, and Y.-C. Kuo, "Ball bearing test-rig research and fault diagnosis investigation," *IET Sci., Meas. Technol.*, vol. 10, no. 4, pp. 259–265, Jul. 2016.
[40] J.-H. Chen, "Controlling chaos and chaotification in the Chen–Lee system by multiple time delays," *Chaos, Solitons Fractals*, vol. 36, no. 4, pp. 843–852, May 2008.
[41] M. Heidari and H. Shamsi, "Analog programmable neuron and case study on VLSI implementation of Multi-Layer Perceptron (MLP)," *Microelectron. J.*, vol. 84, pp. 36–47, Feb. 2019.
[42] Á. Arnaiz-González, A. Fernández-Valdivielso, A. Bustillo, and L. N. L. De Lacalle, "Using artificial neural networks for the prediction of dimensional error on inclined surfaces manufactured by ball-end milling," *Int. J. Adv. Manuf. Technol.*, vol. 83, nos. 5–8, pp. 847–859, Mar. 2016.
[43] S.-H. Oh, "Error back-propagation algorithm for classification of imbalanced data," *Neurocomputing*, vol. 74, no. 6, pp. 1058–1061, Feb. 2011.
[44] T. Hu, Q. Wu, and D.-X. Zhou, "Distributed kernel gradient descent algorithm for minimum error entropy principle," *Appl. Comput. Harmon. Anal.*, to be published.
[45] D. Verstraete, A. Ferrada, E. L. Droguett, V. Meruane, and M. Modarres, "Deep learning enabled fault diagnosis using time-frequency image analysis of rolling element bearings," *Shock Vib.*, vol. 2017, pp. 1–17, Oct. 2017.

CHIH-JER LIN (Member, IEEE) received the B.S., M.S., and Ph.D. degrees from National Cheng Kung University, Tainan, Taiwan, in 1992, 1994, and 1998, respectively, all in mechanical engineering. He is currently a Professor and the Director of the Graduate Institute of Automation and Technology, National Taipei University of Technology, Taipei, Taiwan. His current research interests include mechatronics, precision motion control, system identification, sliding-mode control, robotics, and evolutionary algorithms.

XIAO-YI SU received the B.S. and M.S. degrees from the National Chin-Yi University of Technology, Taichung, Taiwan, in 2017 and 2019, respectively. He is currently pursuing the Ph.D. degree with the College of Mechanical and Electrical Engineering, National Taipei University of Technology. His research interests include nonlinear system analysis and control.

KUAN-TING YU received the B.S. degree from the National Chin-Yi University of Technology, Taichung, Taiwan, in 2018, where he is currently pursuing the M.S. degree in electrical engineering. His research interest includes nonlinear system analysis and control.

BO-LIN JIAN received the B.S. degree from the Department of Electrical Engineering, National Formosa University, in 2009, the M.S. degree in materials science and engineering from the National Taiwan University of Science and Technology, in 2011, and the Ph.D. degree from the Department of Aeronautics and Astronautics, National Cheng Kung University, in 2017.

He is currently an Assistant Professor with the Department of Electrical Engineering, National Chin-Yi University of Technology, Taichung, Taiwan. His current research interests include signal and image processing, machine learning, and control systems.

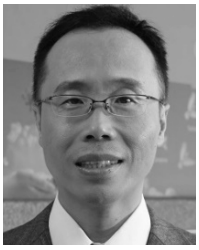

HER-TERNG YAU (Member, IEEE) received the B.S. degree from National Chung Hsing University, Taichung, Taiwan, in 1994, and the M.S. and Ph.D. degrees from National Cheng Kung University, Tainan, Taiwan, in 1996 and 2000, respectively, all in mechanical engineering. He is currently a Professor with the Department of Electrical Engineering, National Chin-Yi University of Technology, Taichung. He is the author of more than 150 research articles in a wide variety of topics in mechanical and electrical engineering. His research interests include energy converter control, system control of mechatronics, and nonlinear system analysis and control.